Ultrasonics Sonochemistry 78 (2021) 105727

Contents lists available at ScienceDirect

Ultrasonics Sonochemistry

journal homepage: www.elsevier.com/locate/ultson

Turning single bubble sonoluminescence from blue in pure water to green by adding trace amount of carbon nanodots

Dan Song [a,b,c], Wen Xu [b,d,e,*], Man Luo [a], Kaijun You [a], Ju Tang [d], Hua Wen [b,c], Xingjia Cheng [b,c], Xiaobing Luo [a], Zhibiao Wang [a,*]

[a] Key Laboratory of Ultrasound in Medicine and Engineering, College of Biomedical Engineering, Chongqing Medical University, Chongqing 400010, China
[b] Key Laboratory of Materials Physics, Institute of Solid State Physics, HFIPS, Chinese Academy of Sciences, Hefei 230031, China
[c] University of Science and Technology of China, Hefei 230026, China
[d] School of Physics and Astronomy, Yunnan University, Kunming 650000, China
[e] Micro Optical Instruments Inc., 518118 Shenzhen, China

ARTICLE INFO

Keywords:
Carbon nanodots
Sonoluminescence
Free radical
Blackbody radiation
Characteristic emission

ABSTRACT

Sonoluminescence (SL) is an interesting physical effect which can convert acoustic energy into light pulses. Up to now, the microscopic mechanism of the SL has not yet been fully clear. It is known that hydroxyl radicals play the important role for SL from water. In this work, we take advantage of carbon nano-dots (CNDs) as free radical captors to modulate the hydroxyl radicals ($OH^{\bullet}$) in SL effect. Through studying the single bubble SL (SBSL) from CND aqueous solution (CNDAS) with trace amount of CNDs, we find that the color of SBSL is tuned dramatically from blue in water to green in CNDAS. Two different SL mechanisms can be identified from emission spectrum. One comes from blackbody-like radiation and another is attributed from the characteristic emission with identified peaks. The decrease in the yield of H_2O_2 in the presence of CNDs suggests the modulation effect on SL via $OH^{\bullet}$ interacting with CNDs. By comparison of the CNDs before and after sonication, it is found that hydroxyl radicals generated during SL can take part in the chain-like oxidation of the chemical groups attached to the CNDs to form larger amount of carboxyl groups. The blackbody temperature of blackbody-like radiation decreases from 15,600 K in water to 11,300 K in CNDAS. Moreover, the emission from hydroxyl radicals and two new luminescent centers related to carboxyl groups are introduced in SL from CNDAS. These important and interesting findings indicate that by adding trace amount of CNDs in water, the effect of SBSL can be significantly modulated, which can provide a macroscopic phenomenon for gaining an insight into the microscopic mechanism of the SL effect.

1. Introduction

Sonoluminescence (SL) has been one of the most important and interesting physical effects in the field of acoustics since the discovery of the multi-bubble SL (MBSL) in 1933 [1] and the single-bubble SL (SBSL) in 1962 [2]. For the case of SBSL, an air or gas bubble in water or solution can be periodically driven by a continuous ultrasonic wave and experience a nonlinear oscillation. With negative and positive acoustic pressures, the bubble can grow and compress then implosively collapse [3]. At the moment of the bubble collapse, a light flash can be generated and such a process can be repeated with the periodicity of the driving acoustic wave [4]. Similar effect can also be observed in multi-bubbles, which is a consequence of the cavitation and the SL induced by the high intensity acoustic wave [5]. The SL is a phenomenon which can take advantage of energy induced from external acoustic wave to generate the light pulses with the width about 100 ps [4]. Meanwhile, the temperature as high as 10^4 K [6], the shock-wave with the pressure up to 4–6 GPa [7] and the fast heating and cooling rates in excess of 10^{12} K/s [5] are accompanied by imploding of the bubble. Therefore, the research field of the SL is very rich in terms of acoustic physics and chemistry. Up to now, the microscopic mechanism of the SL has not yet been fully clear [5,8]. Because the SBSL can provide an ideal and simple case for the

* Corresponding authors at: Key Laboratory of Materials Physics, Institute of Solid State Physics, HFIPS, Chinese Academy of Sciences, Hefei 230031, China (W. Xu). Key Laboratory of Ultrasound in Medicine and Engineering, College of Biomedical Engineering, Chongqing Medical University, Chongqing 400010, China (Z. Wang).
E-mail addresses: wenxu_issp@aliyun.com (W. Xu), wangzb@cqmu.edu.cn (Z. Wang).

https://doi.org/10.1016/j.ultsonch.2021.105727
Received 4 May 2021; Received in revised form 12 August 2021; Accepted 13 August 2021
Available online 25 August 2021
1350-4177/© 2021 The Author(s). Published by Elsevier B.V. This is an open access article under the CC BY-NC-ND license (http://creativecommons.org/licenses/by-nc-nd/4.0/).

generation and detection of the SL, the investigation of SBSL is of great importance and significance in gaining the in-depth understanding of this phenomenon. This becomes our prime motivation in studying the influence of the carbon nanodots (CNDs) in water on SBSL in this work.

The SBSL experiment can be conducted via injecting an air bubble in water around the focal area of an acoustic equipment [9]. It has been found [10,11] that during the process of SBSL, the sonochemical reaction: $H_2O \rightarrow H^{\bullet}+OH^{\bullet}$ can take place, where $H^{\bullet}$ and $OH^{\bullet}$ are respectively the hydrogen and hydroxyl free radicals. Typically, the broadband SBSL from an air bubble in water can be observed from ultraviolet (UV) to about 800 nm wavelength, where the intensity of the light emission decreases with increasing wavelength [9]. Thus, the SBSL from an air bubble in water looks white blue by the naked eyes. Furthermore, for the case of relatively weak driving acoustic field, the characteristic line regarding hydroxyl or $OH^{\bullet}$ can be measured in SBSL spectrum when mixing deionized water with a noble gas (e.g., He, Ar, Xe) [12]. These important experimental findings indicate that hydroxyl or $OH^{\bullet}$ plays an important role in the process of SBSL in water. Now a question one would like to ask is what will happen to SBSL if we make $OH^{\bullet}$ reacts chemically with other matters. To give an example for the answer to this question, in this work we examine how SBSL can be modulated by the presence of carbon-based chemical groups in water.

Carbon nanodots (CNDs), with typical size of several nanometers, are carbon-based nano-materials. They particularly have excellent optical and optoelectronic properties [13–15], versatile features of surface physics and chemistry [16,17] and good water solubility [18]. From a viewpoint of chemistry, CNDs can server as good free radical captors [17] owing to the presence of C-based chemical groups attached to surfaces/edges of the C-cores. In particular, these C-based chemical groups can surely react chemically with $OH^{\bullet}$ generated during the SBSL. In this study, we consider an isolated air bubble levitated acoustically in CNDs aqueous solution (CNDAS) and undertake the SL experiment. We intend studying how the presence of the CNDs in water can affect the SBSL effect. We note that the basic difference of SBSL experiment carried out in a mixture of pure water with the noble gas [12] and in CNDAS is that the noble gas in water normally does not react actively with $OH^{\bullet}$. In this work, we present a comparative study on the SBSL effects in pure water and in CNDAS via measuring the corresponding emission spectra, the time-resolved SL signals and the yields of H_2O_2. We examine the properties of the CNDs before and after sonication, in order to look into the changes bringing to the CNDs during the process of the SL. Thus and conversely, we hope this work can provide some extra information about the features of the SL in water.

2. Samples and experiments

2.1. Synthesis of carbon nanodots

The CNDAS was prepared with the standard hydrothermal method using glucose as precusor. Briefly, 100 mL glucose (2 g), urea (0.2 g), 0.1 M NaOH (10 mL) aqueous solution was heated at 160 ℃ for 12 h in a Teflon-equipped stainless-steel autoclave. After reaction, the solution with CNDs was naturally cooled to room temperature, adjusted to PH = 7 by adding hydrochloric acid. The alkaline solution with small amount of NaOH can speed up the condensation reaction of glucose and improve the synthesis efficiency [19]. Moreover, the added NaOH can lower the oxidation degree of CNDs [20]. Thus, more dangling carbon bonds can be left on the surface/edges of CNDs, which can enhance the ability for CNDs to capture the free radicals. The as-prepared solution with CNDs was filtered with 0.22 μm microporous membrane to remove the large impurities and then dialyzed with a dialysis bag (3000 Da) repeatedly for 6 rounds to remove the small molecules such as NaOH, NaCl, etc. Each round takes about 1 h with newly changed deionized water outside the dialysis bag. Thus, we obtained the CNDAS retained in dialysis bag. Finally the CNDAS was dilute with pure water at volume ratio 1:2. The mass concentration of the as-prepared CNDAS was measured at about 5 g/L. This CNDAS can emit bright blue fluorescence under the UV irradiation.

2.2. The generation and the measurement of sonoluminescence

The experimental setup for single bubble sonoluminescence (SBSL) is shown in Fig. 1. A spherical flask with 130 mm in diameter and two spherical concave ultrasound transducers mounted on two symmetrical sides was filled with pure (deionized and degassed) water or CNDAS (30 mL as-prepared CNDAS was added to 1 L of pure water). Serving as an acoustic resonator, the flask was driven by the acoustic transducer at its fundamental eigen-frequency of 11.6 kHz. The corresponding acoustic pressure around the bubble area was measured by a laboratory-scale needle hydrophone (BT-L-18 M, China Jiliang University) calibrated against a low frequency underwater hydrophone (BK 8103-D-100). Considering more $OH^{\bullet}$ can be generated from a large number of water vapor which diffuses into bubble during the expansion phase [21], a lower frequency was chosen in the present experimental setup compared to previous studies [22]. Thus, the lower frequency in our experiment can benefit the testing of modulation effect on SBSL via $OH^{\bullet}$ interacting with CNDs.

In the experiment, an air bubble was injected into the flask, which can be levitated near the pressure antinode of an acoustic standing wave (close to the center of the flask) [23]. Under the periodic driving of the acoustic wave, the bubble nonlinearly oscillates and emits light pluses. The emission spectrum of SBSL was measured with a spectrometer (IsoPlane SCT320, Princeton Instruments, USA) connected to a photomultiplier (PMT, Hamamatsu R928) through an optical fiber bundle. The spectral resolution is 1 nm in wavelength and the relative irradiance calibration of the spectrometer was undertaken with standard light sources in the wavelength 250–750 nm regime (National Institute of Measurement and Testing Technology, China). The pulses of the light emission from single bubble at the moment of bubble collapse were detected by another PMT (Hamamatsu H7844) and recorded by an oscilloscope. The photographs of sonoluminescing bubble were taken by an electron-multiplying intensified charge-coupled device (emICCD, PI-MAX4-512EM, Princeton Instruments) with an exposure time of 100 ns under back lighting. The photographs of SL from water and from CNDAS were taken by a Nikon D3X digital camera with ISO 6400 and exposure time of 2 s in darkness.

2.3. Enhancement of the sonochemical effect on CNDs

In this work, the SBSL experiment for CNDAS is carried out by adding 30 mL as-prepared CNDAS into l L water in SL apparatus. Therefore, the mass concentration of CNDs in the experiment is very low which is about

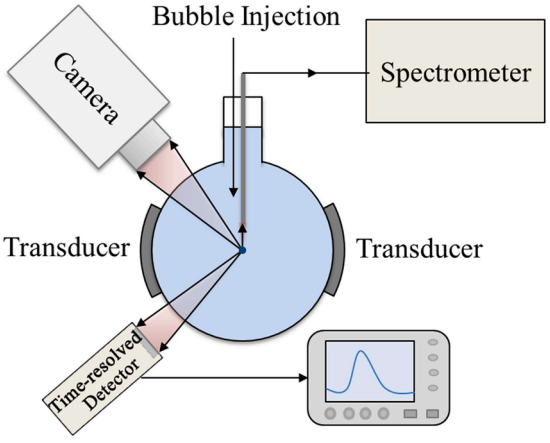

Fig. 1. The experimental setup for single bubble sonoluminescence and related optical measurements.

0.15 g/L. Moreover, in order to enhance the effect of the SL experiment on CNDs for examining the changes of CNDs, we also put the as-prepared CNDAS into a cylindrical Teflon container with a volume of 6 mL and place the container at the focal area of the ultrasound apparatus with a spherical cavity transducer of 480 mm in diameter and 370 mm in height with two axially symmetric open ends. The spherical cavity transducer was immersed in a deionized and degassed water tank withstand a hydrostatic pressure of 10 MPa and was driven by 650 kHz, 630 W acoustic power for 60 s [24,25] (the method to determine the acoustic power is described in Section S1 in Supporting Information). In this way, the cavitation and the SL can take place spontaneously in the focal region and, therefore, the corresponding sonochemical effect can directly and more strongly bring to the CNDs inside the container.

2.4. The evaluation of the yield of hydrogen peroxide induced by sonication

In order to verify further that the $OH^{\bullet}$ generated by SBSL process can be coupled and captured by CNDs, the yields of H_2O_2 in sonicated CNDAS as well as sonicated water were evaluated via UV–Vis absorption using a spectrophotometer (HORIBA JobinYvon). In SL experiment, 12 min sonication was undertaken respectively for CNDAS and for water. Here four samples were prepared as: i) 2 mL pure water used for our experiments was taken as the basis for comparison; ii) 50 μL sonicated water was mixed with pure water to form 2 mL solution; and iii) 50 μL CNDAS before and after sonication were diluted respectively by pure water to form 2 mL solutions. Among above four samples, pure water and CNDAS before sonication are set as blank. The yield of hydrogen peroxide under the effect of sonication can be determined by measuring the absorbance of I_3^- spectrophotometrically in a 1-cm cell using absorptivity $\varepsilon = 26{,}450\ M^{-1}\ cm^{-1}$ at 351 nm [26,27]. The measuring process is described as follows. i) The iodide reagent was prepared by mixing 1 mL of solution A [0.4 M KI, 0.05 M NaOH, 0.00016 M $(NH_4)_6Mo_7O_{24}{\cdot}4H_2O$] and 1 mL solution B [0.1 M $KHC_8H_4O_4$]; ii) 1 mL of each one of four samples mentioned above was added into 2 mL iodide reagent. After mixing, the UV–Vis absorption spectrum of mixed solution was measured (denoted as A_s). iii) The UV–Vis absorption of the reference (denoted as A_r), which was set by adding 2 mL of pure water into 1 mL of each one of four samples, was then measured. iv) The absorbance of I_3^- was deduced via subtracting the spectrum of reference from that of sample, denoted as $\Delta A = A_s - A_r$. Then the value of ΔA at 351 nm was used to evaluate the concentration of I_3^-, which is directly related to the concentration of H_2O_2; v) The H_2O_2 yields in sonicated water and sonicated CNDAS were determined by difference in concentration of H_2O_2 compared with corresponding blank. And vi) considering the dilution rate, the yields of H_2O_2 of original sonicated samples are obtained by multiplying a factor of 40 to the determined value in step v).

2.5. Characterizations

The CNDs before and after sonication were characterized by high-resolution transmission electron microscope (HRTEM, FEI Tecnai G2 TF30) operated at 200 kV, X-ray photoelectron spectroscopy (XPS, PHI 5000 VersaProbe II), ultraviolet–visible absorption spectroscopies (UV–Vis, HORIBA JobinYvon), and photoluminscence (PL) spectroscopy (Jobin Yvon, USA). Through these measurements, we can examine what happens to CNDs due to SL processes.

3. Results and discussions

3.1. Sonoluminescence effect in pure water and CNDAS

3.1.1. The photographs of SL

The photographs of sonoluminescing bubble at its maximum radius, the SL in water and the SL in CNDAS are shown respectively in the left, middle and right panels in Fig. 2. The maximum diameter of sonoluminescing bubble is around 100 μm, which is much larger than the size of CNDs (several nanometers as shown in Section 3.2). Therefore, the presence of CNDs in water does not affect the bubble oscillation significantly so that SL can still be generated in CNDAS, as shown in the right panel in Fig. 2. It should be noted that in our experiments, the spatial location of sonoluminescing bubble around the focal spot is a bit random, similar to those reported by other groups [28,29]. This effect is more obvious in the photos of SL with a shorter exposure time of 0.62 s (see Fig. S1 in Supporting Information). It implies that the sonoluminescing bubble is moving at least translationally under the driving acoustic field [28]. We find that when taking the exposure time to be longer than 2 s, the areas of the SL images for water and for CNDAS can be rather stably observed. Since the frequency of driving acoustic wave is 11.6 kHz and the exposure time for SL photographs is 2 s, the results shown in Fig. 2 come from accumulation for about 23.2 k SL events. It can be seen that SL from CNDAS covers a larger area than that from water, corresponding to the larger bubble transitional movement in CNDAS. From Fig. 2, we notice that the center region of SL in both water and CNDAS looks white which seems a bit saturated. While the color of outer region of SL looks blue for SL from water and looks green to yellow for SL from CNDAS. The obvious influence of the CNDs in water on SL can be observed even by the naked eye. By more carefully checking, we find that the outer region of SL spot in water and in CNDAS looks green. This is owing to the fact that the photos were taken outside the spherical flask, where the refraction of water and the interface of spherical flask can lead to dispersion effect. However, the actual color of SL can be identified more clearly from the SL spectra (as shown in Fig. 4). The intensities of the light pulses as a function of time are shown as insets in Fig. 2 (b) and (c) respectively for SL from water and from CNDAS. As can be seen, the periodicity of the SL pulses from both water and CNDAS is stably in consistent with the frequency of the driving acoustic wave, whereas the intensities of SL pulses can be deviated.

In this study, the acoustic pressure around the bubble area was measured to be about 1.19 atm. This condition is around the border area between stable SBSL and dancing region (bubble undergoes a non-destructive shape instability identified in literature as a "jittering state'', in this case, the bubble is translationally moving from the focal spot) [30,31], as being pointed out and demonstrated theoretically [32]. This is the main reason why the asymmetrical SL spots, the translational movement of the sonoluminescing bubble and the deviation of the pulse intensities can be observed for SBSL from pure water and from CNDAS.

3.1.2. The time-resolved SL pulses

The time-resolved intensity signals of SL pulses from water (blue dotted curve) and from CNDAS (red dotted curve) are shown in Fig. 3, where the green dotted curve is the time resolution response of the measurement system, obtained under an extremely dark condition via single photon response measurement. The obvious difference between the resolution response of the measurement system (green dotted curve) and the measured SL pulses (blue and red dotted curves) suggests that the measured SL signals do present the features of time evolution for the SL processes. The full width of the SL pulse from water (CNDAS) is 20.31±0.18 ns (22.38±0.09 ns). We find that the full width of SL from CNDAS is larger than that from water. The decay slopes of the SL intensity signals can fit nicely with the exponential functions for SL emission from water (magenta solid curve) and from CNDAS (black solid curve) respectively. Through fitting, we find that the decay time for SL from water (from CNDAS) is 6.7 ns (7.8 ns). The decay of SL from CNDAS is slight slower than that from water. This implies that the strength of the light emission during the collapse of bubble or the emission species are different in two cases [33]. Moreover, we know that the decay time of PL emission from CNDs is normally about 10 ns [30,31] (also see Fig. S2 in Supporting Information). It is much longer than pulse duration of the SL (about 100 ps) [6]. If the PL from CNDAS can be taken as the input of the measurement system (PMT), the output is significantly different from SL

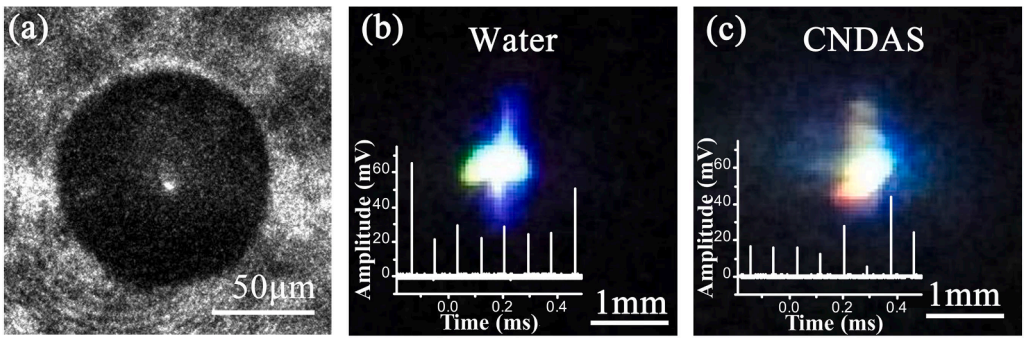

Fig. 2. Photographs of sonoluminescing bubble at its maximum radius (left panel), SL in water (middle panel) and in CNDAS (right panel). The intensities of the light pulses as a function of time are shown in insets in (b) and (c) respectively for SL from water and CNDAS.

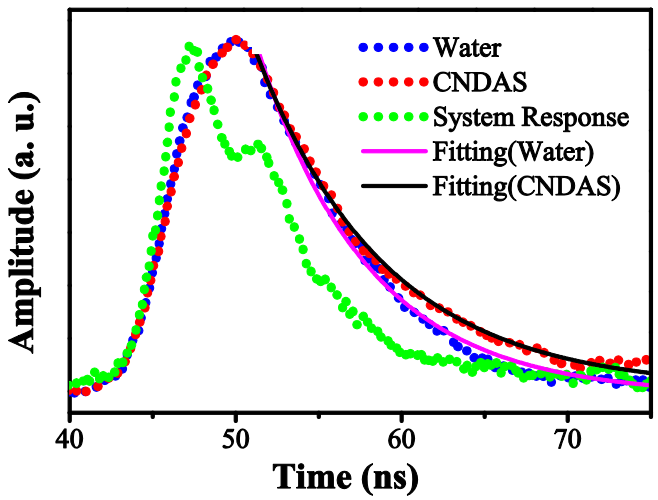

Fig. 3. The intensity of the SL pulses from pure water (blue dotted curve) and from CNDAS (red dotted curve) as a function of time. The corresponding decay slopes are fitted exponentially with a decay time of 6.7 ns (magenta solid curve) for SL from pure water and of 7.8 ns (black solid curve) for SL from CNDAS. The green dotted curve is the time resolution response of the measurement system. (For interpretation of the references to color in this figure legend, the reader is referred to the web version of this article.)

from CNDAS (also see Fig. S3 in Supporting Information). Since we do not observe the difference in decay time between SL from water (blue dotted curve in Fig. 3) and from CNDAS (red dotted curve in Fig. 3), the mechanism that the light emission from CNDAS is induced by the PL from CNDs pumped by UV-blue radiation from SL is not dominate in our experiment and observations. Thus, the red dotted curve in Fig. 3 should be the result of SL directly from CNDAS.

3.1.3. SL spectra

The spectra of SL from water and from CNDAS are shown in upper and lower panels of Fig. 4, respectively. It should be noted that the optical absorption of CNDAS has been subtracted out from measured SL spectrum, where the UV–Vis absorption spectrum of CNDAS with thickness of 10 mm and a dilution rate of 10% is shown in the lower panel of Fig. 6. According to the Lambert-Beer law [35], the relationship between the absorbance (A) and the transmittance (T) for CNDAS is given as:

$$A = \lg\left(\frac{I_0}{I_t}\right) = \lg\left(\frac{1}{T}\right) = \varepsilon bc, \quad (1)$$

where ε, b and c are respectively the absorptivity, the thickness and the concentration of absorption medium (*e.g.*, CNDs in our case). From this

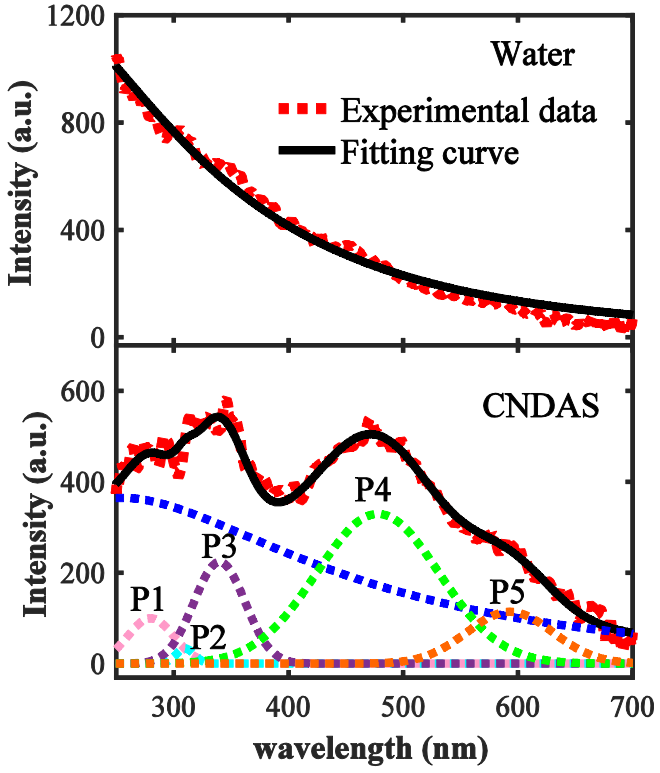

Fig. 4. The SL spectra from pure water (upper panel) and from CNDAS (lower panel). Here, the experimental data are presented by red dotted curves and the fitting curves are presented as black solid curves. The SL spectrum from pure water can be fitted by blackbody radiation, while that from CNDAS can be fitted with a combination of blackbody radiation (blue dotted curve) and Gaussian curves (pink, cyan, purple, green and orange dotted curves labeled by peak positions P1 to P5). (For interpretation of the references to color in this figure legend, the reader is referred to the web version of this article.)

relationship, the transmittance of CNDAS with a thickness of 5 mm (i.e., the distance from optical fiber tip to the position of sonoluminescing bubble) and a dilution rate of 3 % in SBSL experiment can be obtained (see Fig. S4 in Supporting Information). Thus, the effect of optical absorption by CNDAS can be subtracted out.

As shown in Fig. 4, the intensity of SL from water (upper panel) decreases monotonously with increasing wavelength, which is a typical SBSL spectrum from pure water [6]. As for the case of CNDAS (lower panel), two obvious peaks and one kink-like shoulder can be observed in the emission spectrum. It is well known that the SL spectrum comes mainly from mechanisms such as plasma-like emission and emission from excited species like $OH^{\bullet}$ [36]. In Fig. 4, the SL spectrum from water

and the main parts of that from CNDAS can be fitted by blackbody radiation formula [6], which implies it comes plasma-like emission. In SL spectrum from CNDAS, the kink-like shoulders and the peaks can be decomposed by Gaussian fittings [37] due to emission from excited species. Thus, the SL spectra can be fitted by a combination of blackbody radiation and Gaussian like characteristic emission via:

$$P(\lambda) = \frac{a}{\lambda^5\left[\exp\left(\frac{hc}{\lambda k_B T_b}\right) - 1\right]} + \sum_{n=1} a_n \exp\left[\frac{-(\lambda-\lambda_n)^2}{2b_n{}^2}\right], \quad (2)$$

where $P(\lambda)$ is the spectral irradiance at a wavelength λ, a is the fitting coefficient for irradiance from blackbody radiation, T_b is the blackbody temperature, and h, c and k_B are the Planck's constant, the speed of light and the Boltzmann constant, respectively. Furthermore, a_n, b_n and λ_n are fitting parameters for the n^{th} characteristic emission center. For SL from pure water, there is no obvious characteristic emission. Thus, we take only the first term in Equation (2) to achieve a good fitting.

From Fig. 4, we see that the SL from water is stronger than that from CNDAS in the measured wavelength regime. Through fitting, we obtain the blackbody temperature for SL from pure water to be at about 15600 K and from CNDAS at about 11300 K. In our experiment, we find that there is a kink-like shoulder and two peaks in the emission spectrum of CNDAS. They are probably associated with characteristic light emission from excited species (e.g. OH•). Through Gaussian fitting, the kink-like shoulder and the peaks associate with characteristic emission in the spectrum from CNDAS are analyzed.

It is well known that OH •radicals can be formed in sonolysis of water via reaction [22,38]:

$$H_2O \rightarrow OH^{\bullet} + H^{\bullet}. \quad (3)$$

They are the dominate radicals for sonolysis of air bubble SL in pure water, compared with other generated species such as HNO_3 and HNO_2 [39]. In Fig. 4, The high frequency peak can be deconvoluted into three Gaussian curves (P1, P2 and P3) with peak wavelength located at 280 nm, 310 nm and 340 nm, which are associated with 0–1, 0–0 and 1–0 vibrational transition of the electronic transition channel $A^2\Sigma^+ \rightarrow X^2\Pi$ in OH•, respectively [11,40]. The light emission from OH• usually has its maximum at 310 nm [12,41]. The emission peak from OH• at 280 nm and 340 nm can also be identified obviously in SL experiments by many groups [11,40,42]. In our experiment, the light emissions around 280 nm and 340 nm are much stronger than the emission around 310 nm which cannot be clearly identified in experimental spectrum, although the peak at 310 nm can be decomposed theoretically (see cyan dotted curve in lower panel of Fig. 4). Such a feature can be attributed to the coupling of CNDs with hydroxyl radicals. The emission around 340 nm can also come from NH as reported by R. Pflieger, et al. [43]. Because the possibility for OH• $A^2\Sigma^+ \rightarrow X^2\Pi$(v:1–0) transition is relatively low, a more reasonable mechanism for strong emission at 340 nm shown in Fig. 4 is mainly attributed to NH arising from traces of air and from N-related groups attached to CNDs (see XPS results shown in Fig. S5 in Supporting Information). In low frequency regime, we find that the peak and the kink-like shoulder for SL from CNDAS are at about 478 nm and 593 nm, respectively, which can be fitted with another two Gaussian curves (P4 and P5). The main difference of SBSL from water and from CNDAS can be understood with the help of the results obtained from characterization of CNDs before and after sonication.

3.2. The characterization of CNDs before and after sonication

The HRTEM results of CNDs before and after sonication are shown in Fig. 5. The CNDs after sonication distribute more uniformly in the imaging region. The average size of carbon core of CNDs before sonication (4.4 ± 0.9 nm) is larger than that of CNDs after sonication (3.6 ± 0.8 nm). It should be noted that before sonication the CNDs is heavily agglomerated. From TEM images we can only identify several isolated carbon cores (sample size: 11 particles) to evaluate the average size of the CNDs. Thus, the histogram cannot be given statistically in Fig. 5(a). The obvious lattice spacing with lattice constants of 0.246 nm can be identified in CNDs before sonication, shown in Fig. 5(a), which is close to the lattice constants of (1120) facet of graphite [44]. In Fig. 5(b), the obvious lattice structures with spacing of 0.21 nm can be observed in CNDs after sonication corresponding to the (1 0 0)-facet spacing of the graphite [45]. These results indicate that, after being treated by the SL experiment, the CNDs have a smaller average size. The main reason is that the mechanical effect of the acoustic vibration and/or launched shock-wave from collapsed bubble can make CNDs smaller and more uniformly distributed.

The XPS results show that there are mainly three kinds of atoms such as C, O, and N in CNDs both before and after SL experiment (see Fig. S5 in Support Information). Among these atoms, the nitrogen content decreases while oxygen content largely increases in CNDs after SL experiment. The oxygen content in CNDs after sonication is much larger (31.69 %) than that before treated (26.19 %). The O1s spectra are shown in Fig. 6 (a), which can be deconvoluted into the contributions from C=O (530.9 eV), -O-C=O (532 eV) and C-O (533.2 eV) [46]. The types and contents of chemical bonds deconvoluted from C1s spectra as well as O1s spectra of CNDs before (blue bar) and after (red bar) sonicated are demonstrated with bar graph as shown in Fig. 6(b). The value of R-square is 0.9989 (0.9961) for C1s spectra fitting for CNDs before (after) SL experiment. And the value of R-square is 0.9979 (0.9972) for O1s spectra fitting for CNDs before (after) sonication. In the bar graph of chemical bonds deconvoluted from O1s, the first column refers to chemical bond of C-O only. From Fig. 6(b), we note that after sonication, there are larger contents of chemical bonds -O-C=O, which refer to chemical groups of –COOH, and smaller contents of C-O (including C-O

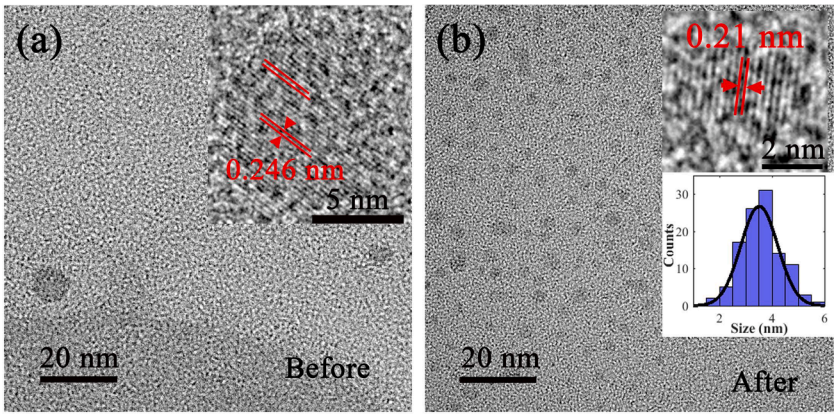

Fig. 5. HRTEM images of CNDs (a) before and (b) after sonication. The high resolution images of the carbon cores and the size histogram are shown in the insets.

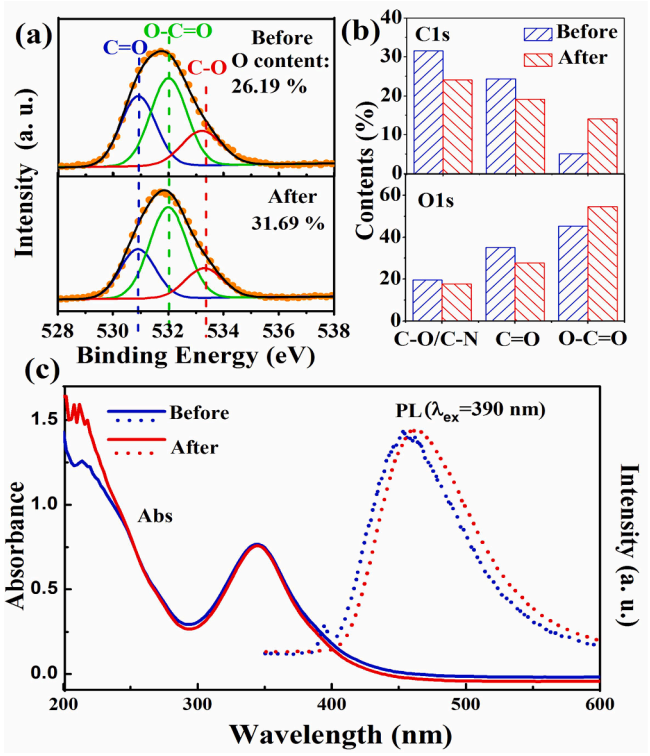

Fig. 6. (a) XPS O1s spectra of CNDs (orange dots) before (upper panel) and after (lower panel) sonication, which can be deconvoluted into the contributions from C=O (530.9 eV, blue curve), -O-C=O (532 eV, green curve) and C-O (533.2 eV, red curve). The cumulative of these contributions is illustrated by black curve. (b) The types and contents of chemical bonds deconvoluted from C1s spectra (upper panel) and from O1s spectra (lower panel) for CNDs before (blue bar) and after (red bar) sonication. In the lower panel, the first column refers to C-O only. (c) The UV–Vis absorbance spectra of CNDs before (blue solid curve) and after (red solid curve) sonication, along with their PL spectra excited by wavelength of 390 nm (dotted curves). (For interpretation of the references to color in this figure legend, the reader is referred to the web version of this article.)

bond from hydroxl and hydroxymethyl groups) and C=O (including C=O bond from ketone and aldehyde groups) in CNDs. These results indicate that oxidizing reactions to CNDs take place during sonication.

The PL (solid curves) and the UV–Vis absorption (dotted curves) spectra of CNDs are shown in Fig. 6(c), where the results for CNDs before and after sonication are illustrated by blue and red curves, respectively. The peak located at 345 nm in UV–Vis absorption spectra corresponding to n-π* transition introduced by chemical groups attached to the surfaces/edges of carbon cores. The peak of the PL emission from CNDs before (after) sonication is located at about 452 nm (461 nm), measured at an excitation wavelength of 390 nm. We notice that after sonication, the red-shifts of PL spectrum can be observed. It has been demonstrated that larger contents of –COOH groups on CNDs can lead to a narrower band gap between n and π* orbitals [45]. This is the main reason why the red-shift of PL can be observed for CNDs after sonication, in consistent with the results obtained from XPS.

3.3. The comparison of H_2O_2 yields in sonicated water and CNDAS

As a secondary product of OH• recombination, the yield of H_2O_2 is directly related to the amount of OH• in a water based solution. In the presence of H_2O_2, oxidation to iodide reagent takes place to form I_3^-. The corresponding chemical reactions are:

$$OH\bullet + OH\bullet \rightarrow H_2O_2, \quad (4)$$

$$H_2O_2 + 2I^- + 2H^+ \rightarrow I_2 + 2H_2O, \quad (5)$$

$$I_2 + I^- \rightarrow I_3^-. \quad (6)$$

The absorption spectra of I_3^- for four samples (pure water, sonicated water, and CNDAS before and after sonication) are shown in Fig. S6 in Supporting Information. Applying the Lambert-Beer low [35] (see Equation (1)) as $A = \varepsilon bc$, where the absorptivity of I_3^- is $\varepsilon = 26{,}450\ M^{-1}\ cm^{-1}$ [27] and the thickness of absorption medium b is 1 cm, we can determine the value of c which is the concentration of I_3^-. For the case of water before and after sonication, I_3^- ions are mainly generated by H_2O_2 so that we can obtain the concentration of H_2O_2 through the concentration of I_3^-. We note that this method is valid for measuring H_2O_2 yield in water [26]. For the case of CNDAS, there has been no easy and direct way to measure the H_2O_2 yield in CNDAS so far. The main reason is that the iodide reagent can react with CNDs via surface oxidation [47] and the absorption peak of CNDAS is at 345 nm (see Fig. 6) which overlaps largely with that of I_3^- at 351 nm. However, the influence of optical absorption by CNDAS can be eliminated via background subtracting with the spectrum of reference. After assuming that the reaction between iodide reagent and CNDs via surface oxidation is relatively weak, the yield H_2O_2 in CNDAS can be roughly evaluated.

Following the method described in section 2.4, the yield of H_2O_2 in sonicated water (CNDAS) is 66.5 μM (1.9 μM). It reveals that the yield of H_2O_2 concentration in sonicated CNDAS is dramatically smaller than that in sonicated water. The main reason behind this is that the hydroxyl radicals are captured by CNDs before their self-recombination to form H_2O_2. The more OH• are captured by CNDs, the smaller yield of H_2O_2 in sonicated CNDAS can be achieved. This observation supports further to our proposal that the modulation to SBSL by the presence of CNDs is mainly achieved via interaction of CNDs with OH• generated during the SL process.

3.4. The effect of the presence of CNDs on SL

According to the theory for interactions between a bubble and a particle, proposed by Gail Ter Haar and co-workers [48], the force induced by an acoustically driven bubble on a particle can be described as:

$$\boldsymbol{F_p} = \frac{4\pi\rho_0|A|^2 R_{b0}{}^2 R_p{}^3}{L^5\left[\left(1-\omega_{b0}{}^2/\omega^2\right)^2+\delta_b{}^2\right]}\left(\frac{\rho_p-\rho_0}{\rho_0+2\rho_p}\right)\boldsymbol{e_p}, \quad (7)$$

where A and ω are the pressure strength and the frequency of the driving acoustic wave, R_{b0} is the equilibrium radius of bubble, R_p is the radius of the particle, $\omega_{b0} = \sqrt{3\gamma p/\rho_0 R_{b0}{}^2}$ is the fundamental resonant frequency of the bubble with γ, p and ρ_0 being respectively the specific heat ratio, the hydrostatic pressure and the density of the host liquid, δ_b is the damping constant of the bubble, L is the distance between the bubble and the particle with a density ρ_p, and $\boldsymbol{e_p}$ is a direction vector with origin at the center of the particle and pointing to the bubble. Form this equation, we see that when $\rho_p > \rho_0$, the force $\boldsymbol{F_p} > 0$ so that the particle is attracted by the bubble [49]. In our present case, the particle is the CND and the host liquid is water. Because the density of a CND is usually larger than that of water, the CNDs in water are attracted by the bubble in the presence of acoustic radiation force. Thus, the CNDs in water can gather to the bubble, which provides a basic condition for CNDs to affect the SL even for the case where the trace amount of CNDs are presented in water.

From XPS results (see Fig. 6(a) and Fig. 6(b)), we know that after experienced the SL experiment, significant changes have been introduced to CNDs. Except for the changes of the carbon core which are mainly induced by the mechanical and thermal effects during the SL, the chemical groups attached to the surfaces/edges of CNDs have also been altered. The content of –COOH groups attached to the surfaces/edges of

CNDs is increased, while the contents of –OH and -C=O groups are reduced. This indicates that the oxidation to the CNDs takes place during the SL experiment. As we know, the sonolysis of water is the most common reaction during SL, which leads to the formation of highly oxidizing hydroxyl radicals via the reaction described in Equation (3). It should be pointed out that during the sonolysis process for an air bubble in water, oxidizing species of HNO_3 can also be generated with a relatively smaller yield than hydroxyl [39]. While the oxidation to CNDs can only be achieved with a relative high concentration of HNO_3 and longer action time of sonication [50]. Moreover, the dramatically decrease in the yield of H_2O_2 in CNDAS is a direct evidence to chemical reaction between $OH^{\bullet}$ and CNDs. Thus, the oxidation to the CNDs is mainly induced by $OH^{\bullet}$. With the participation of $OH^{\bullet}$, $–CH_2OH$ and –CHO groups on CNDs can be oxidized to form –CHO and –COOH groups respectively, as described in upper region of Scheme 1.

As shown in Fig. 4, the characteristic SL peaks at 478 nm and 593 nm are induced by the presence of CNDs in water. They must be the consequence of the chemical reactions during the SL process. We note that similar to SL from pure water, the SL spectrum from CNDAS can also be repeatedly measured. This feature suggests that the chemical reactions to CNDs during SL are most likely reversible. Thus, new luminescence centers which generate the characteristic light emission at 478 nm and 593 nm are most likely associated with the final products of chain-like oxidation reactions, that is –COOH groups suggested by the XPS results. Here, we discussed possible mechanisms for how CNDs take part in the sonoluminescence process. We notice that the characteristic light emission in SBSL from nonvolatile species (e.g., Na^+) can be induced by the Injected Droplet & Jet Model [51]. Under the action of intense acoustic pressure (i.e., 5.4 atm in [32]), the nonvolatile species can enter into the bubble when the macroscopic bubble movement becomes chaotic and, thus, entrain liquid droplets in the bubble interior [51]. In our experiment, the acoustic pressure is only 1.19 atm and the average size of CNDs (several nm) is much larger than that of ions such as Na^+. As a result, the characteristic SL from CNDAS in this study is less possibly caused by the Injected Droplet & Jet Model. Based on our results for SBSL from CNDAS and for characterization of CNDs before and after sonication, we believe that carboxylate radicals can be isolated from the carbon cores of CNDs under the attack of free hydroxyl radical generated during SL [52]. The carboxylate radicals with small molecule weight can take part in the SL process and introduce new centers for characteristic light emission through diffusive and chemical processes of mass exchange between bubble and liquid.

From Fig. 4, we learn that in the presence of CNDs, two major emission channels coexist in SL process, one comes from blackbody-like radiation and another is attributed from the characteristic emission with

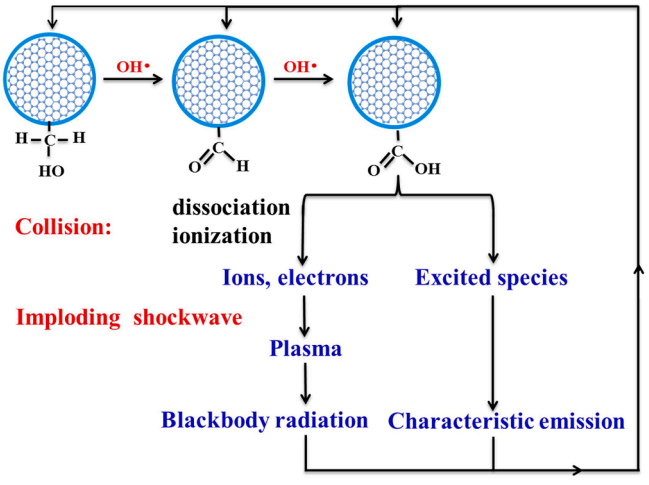

Scheme 1. The flow chart for SL emission from CNDAS and the related chemical reactions.

identified peaks. The mechanism for continuous or blackbody radiation can be understood as follows. As we know, during bubble collapsing, the volume of the bubble is rapidly reduced and the energy maintaining inside the bubble becomes highly condensed. The violent collapse of the bubble can lead to the generation of the shock wave with a velocity of about 4000 m/s from the bubble wall [7,53]. In the presence of CNDs in water, the high energy release and the strong inward shock-wave during can accelerate the carboxylate radicals to gain high kinetic energy. The collision of these highly accelerated carboxylate radicals with other molecules in water can result in the dissociation of the chemical bonds to form smaller molecules or atoms. Moreover, if the energy gain is larger than the ionization energy of the carboxylate radicals or its dissociated products, ions and free electrons can be induced. With the on-going implosion of the bubble, the inward shock-wave can confine the ions and free electrons to form the plasma. The spectrum of the plasma is continuous and its wavelength dependence relates to the temperature or energy of the plasma. From Fig. 4, we see that the blackbody-like radiation from CNDAS is relatively weaker than that from water and the corresponding blackbody temperature is lower. The main reasons behind these features are: 1) the presence of CNDs can lead to larger movement and decrease in spatial stability of sonoluminescing bubble, corresponding to the larger area of SL emission (see Fig. 2); 2) with the presence of carboxylate radicals, more endothermic chemical reactions are introduced to the imploding process. Thus, more energy generated is consumed by endothermic chemical reaction and less energy can be converted to SL emission; 3) the presence of CNDs introduce emitting species with larger mass than hydroxyl radicals, which lead to the decrease of velocity after collision and the kinetic energy of the emitting species. On the other hand, the mechanism for characteristic SL emission in the spectrum can be described as following. The presence of CNDs and their interaction with $OH^{\bullet}$ can introduce new centers for light emission with distinguishable peaks related to specific type of luminescent species. The collision of highly accelerated carboxylate radicals can also pump electrons in carboxylate radicals into higher energy states. This process is allowed by the momentum and energy conservation laws for electronic collision events. The radiative relaxation of these electrons can generate the characteristic radiation in the SL spectrum. After bubble collapsing and SL, the free radicals from de-excited species and ions are captured back by the carbon core of CNDs to form various chemical groups on CNDs. These groups are mainly carboxyl-based, owing to the presence of hydroxyl radicals. Hence, two reversible channels of excitation and radiation for, respectively, the blackbody-like radiation and characteristic emission are presented simultaneously for SL from CNDAS, which can be illustrated as Scheme 1.

According to the wavelengths of characteristic SL from CNDAS (see Fig. 4), we can look into the possible luminescent centers for these emission, in conjunction with the results obtained from the characterization of CNDs before and experienced the SL. From above presented discussions, we believe that CO-based molecule is most likely the one which can contribute the characteristic SL peaked at 478 nm and 593 nm. The electronic energy levels in CO molecule are known [54]. In particular, the Ångstrom system ($B^1\Sigma^+ \rightarrow A^1\Pi$) of the CO molecular covers the wavelength range from 440nm to 560nm [55]. The SL peak at 478 nm may come from this electronic transition channel. Similar broadband emission from CO molecular has been reported by Pflieger et al. in SL at high acoustic driving frequency [56]. It is expected that better resolution of the emission lines from a molecular can be achieved at a low driving frequency [43]. In this study, the spectral resolution of the spectrometer is 1 nm which is not high enough to reveal the fine structure of SL spectrum. It is also known that the transition bands ($d^3\Delta^+ \rightarrow a^3\Pi$) in CO is a series of spectral line ranging from about 550 nm to about 900 nm [54,57]. The SL peak at 593 nm may come from this electronic transition channel. It should be noted that the $A^1\Pi$ and $d^3\Delta^+$states of CO are often perturbed by other occupied or valence states. As a results, they are normally split and form the broadened

energy band [55,58]. This is one of the reasons why the broadened peaks in SL spectra can be observed in Fig. 4. Furthermore, the excited states $B^1\Sigma^+$and $d^3\Delta^+$in CO molecule are about 11 eV and 6 eV from the ground state, respectively, which are much higher than the thermal energy estimated from blackbody radiation. Hence, the excited states $B^1\Sigma^+$and $d^3\Delta^+$in CO are less possibly thermally populated. As a result, the electronic population of these excited states in CO is mainly induced by collision interaction with high energy particles [59]. The electronic transitions from the excited states to the ground state in CO, such as ($A^1\Pi \rightarrow X^1\Sigma^+$), are allowed in principle. However, they are in the deep UV regime [54] which is beyond our measurement range in the present study.

4. Conclusions

In this work, we have studied a new phenomenon of SL by adding trace amount of CNDs in water. It has been found that the presence of CNDs in water can turn blue SBSL from pure water into green. To understand this interesting and important phenomenon, we have performed the related characterization measurements to examine what happens to CNDs after experienced the SL experiment. The main conclusions drawn from this study can be summarized as follows.

Similar to SBSL from pure water, SBSL can be observed repeatedly in CNDAS. The area of SBSL from CNDAS is larger than that from water and the colors of the SL are obviously different in two cases. Moreover, the characteristic peaks can be clearly observed in SL spectrum from CNDAS.

We have found that SL spectrum from CNDAS can be considered as combination of broad continuous radiation and characteristic emission. The former case can be fitted by the blackbody radiation formula and the latter case can be described by multiple Gaussian fitting. They come from different channels for electronic excitation and radiation. The former case is mainly induced by plasma which is generated via collision-induced ions and electrons during the collapse of the bubble. The latter case is mainly attributed from electronic relaxation within the energy states in OH radical or CO molecule, where the effect of collision plays a role as electronic pumping.

The SL from water is stronger than that from CNDAS, especially in short wavelength regime. Via fitting, we have found that the blackbody temperature for SL from water is about 15,600 K, which is much higher than 11,300 K measured for SL from CNDAS. Except emission from hydroxyl radicals, the characteristic SL emissions in CNDAS are mainly induced by carboxyl groups attached to the surfaces/edges of nanocarbon core, which come from CO molecule dissociated from carboxyl groups.

The results obtained from this work can provide us a rather clear picture about how the presence of CNDs in water can modulate the SL effect. This can be helpful in gaining an insight into the microscopic mechanism of SL effect.

CRediT authorship contribution statement

Dan Song: Data curation, Formal analysis, Writing – original draft, Writing – review & editing, Conceptualization. **Wen Xu:** Conceptualization, Supervision, Methodology, Writing – review & editing. **Man Luo:** Data curation, Formal analysis. **Kaijun You:** Validation, Methodology. **Ju Tang:** Methodology, Formal analysis. **Hua Wen:** Software. **Xingjia Cheng:** Visualization. **Xiaobing Luo:** Investigation. **Zhibiao Wang:** Resources, Supervision, Project administration.

Declaration of Competing Interest

The authors declare that they have no known competing financial interests or personal relationships that could have appeared to influence the work reported in this paper.

Acknowledgment

Our sincere thanks to Prof. Mingming Guo, Yuran Tang and Prof. Jing Zhang for providing help on sample characterization.

Funding

This work was supported by the National Natural Science foundation of China (81127901, U206720039, U193010069) and by Shenzhen Science and Technology Program (KQTD20190929173954826).

Appendix A. Supplementary data

Supplementary data to this article can be found online at https://doi.org/10.1016/j.ultsonch.2021.105727.

References

[1] N. Marinesco, J.J. Trillat, Action des ultrasons sur les plaques photographiques, C. R. Acad. Sci. Paris. 196 (1933) 858.
[2] K. Yosioka, A. Omura, The light emission from a single bubble driven by ultrasound and the spectra of acoustic oscillations, Proc. Annu. Meet. Acoust. Soc. Jpn. (1962) 125–126.
[3] B.P. Barber, S.J. Putterman, Light scattering measurements of the repetitive supersonic implosion of a sonoluminescing bubble, Phys. Rev. Lett. 69 (1992) 3839–3842.
[4] B.P. Barber, S.J. Putterman, Observation of synchronous picosecond sonoluminescence, Nature. 352 (1991) 318–320, https://doi.org/10.1038/352318a0.
[5] K.S. Suslick, N.C. Eddingsaas, D.J. Flannigan, S.D. Hopkins, H. Xu, The chemical history of a bubble, Acc. Chem. Res. 51 (2018) 2169–2178, https://doi.org/10.1021/acs.accounts.8b00088.
[6] R. Hiller, S.J. Putterman, B.P. Barber, Spectrum of synchronous picosecond sonoluminescence, Phys. Rev. Lett. 69 (1992) 1182–1184, https://doi.org/10.1103/PhysRevLett.69.1182.
[7] R. Pecha, B. Gompf, Microimplosions: cavitation collapse and shock wave emission on a nanosecond time scale, Phys. Rev. Lett. 84 (2000) 1328.
[8] M.P. Brenner, S. Hilgenfeldt, D. Lohse, Single-bubble sonoluminescence, Rev. Mod. Phys. 74 (2002) 425–484, https://doi.org/10.1103/RevModPhys.74.425.
[9] D.F. Gaitan, Sonoluminescence and bubble dynamics for a single, stable, cavitation bubble, J. Acoust. Soc. Am. 91 (1992) 3166–3183.
[10] Y.T. Didenko, W.B. McNamara III, K.S. Suslick, Molecular emission from single-bubble sonoluminescence, Nature 407 (2000) 877–879, https://doi.org/10.1038/35038020.
[11] R. Pflieger, H.P. Brau, S.I. Nikitenko, Sonoluminescence from OH(C2Σ+) and OH(A 2Σ+) radicals in water: evidence for plasma formation during multibubble cavitation, Chem. - A Eur. J. 16 (2010) 11801–11803, https://doi.org/10.1002/chem.201002170.
[12] J.B. Young, J.A. Nelson, W. Kang, Line emission in single-bubble sonoluminescence, Phys. Rev. Lett. 86 (2001) 2673–2676, https://doi.org/10.1103/PhysRevLett.86.2673.
[13] K.J. Williams, C.A. Nelson, X. Yan, L.-S. Li, X. Zhu, Hot electron injection from graphene quantum dots to TiO2, ACS Nano 7 (2013) 1388–1394, https://doi.org/10.1021/nn305080c.
[14] L. Tang, R. Ji, X. Li, G. Bai, C.P. Liu, J. Hao, J. Lin, H. Jiang, K.S. Teng, Z. Yang, S. P. Lau, Deep ultraviolet to near-infrared emission and photoresponse in layered n-doped graphene quantum dots, ACS Nano 8 (2014) 6312–6320, https://doi.org/10.1021/nn501796r.
[15] Z. Zhu, J. Ma, Z. Wang, C. Mu, Z. Fan, L. Du, Y. Bai, L. Fan, H. Yan, D.L. Phillips, S. Yang, Efficiency enhancement of perovskite solar cells through fast electron extraction: the role of graphene quantum dots, J. Am. Chem. Soc. 136 (2014) 3760–3763, https://doi.org/10.1021/ja4132246.
[16] M. Lu, L. Zhou, One-step sonochemical synthesis of versatile nitrogen-doped carbon quantum dots for sensitive detection of Fe~(2+) ions and temperature in vitro, Mater. Sci. Eng. 101 (2019) 352–359.
[17] F. Li, T. Li, C. Sun, J. Xia, H. Xu, Selenium-doped carbon quantum dots (Se-CQDs) for free radical scavenging, Angew. Chem. - Int. Ed. 56 (2017) 9910–9914, https://doi.org/10.1002/anie.201705989.
[18] J. Zhang, H. Wang, Y. Xiao, J. Tang, C. Liang, F. Li, H. Dong, W. Xu, A simple approach for synthesizing of fluorescent carbon quantum dots from tofu wastewater, Nanoscale Res. Lett. 12 (2017) 611.
[19] H.C.M. Pijnenburg, B.F.M. Kuster, H.S. van der Baan, The simultaneous isomerization and hydrogenation of glucose in alkali solutions, Starch - Stärke. 30 (1978) 199–205, https://doi.org/10.1002/star.19780300606.
[20] L. Zhao, F. Di, D. Wang, L.H. Guo, Y. Yang, B. Wan, H. Zhang, Chemiluminescence of carbon dots under strong alkaline solutions: a novel insight into carbon dot optical properties, Nanoscale 5 (2013) 2655–2658, https://doi.org/10.1039//b000000x.
[21] J.-S. Jeon, J.-Y. Lee, H.-Y. Kwak, Possibility of upscaling for single bubble sonoluminescence at a low driving frequency, J. Phys. Soc. Japan 72 (2003) 509–515, https://doi.org/10.1143/JPSJ.72.509.

[22] Y.T. Didenko, K.S. Suslick, The energy efficiency of formation of photons, radicals and ions during single-bubble cavitation, Nature 418 (2002) 394–397, https://doi.org/10.1038/nature00911.1.
[23] T.J. Matula, S.M. Cordry, R.A. Roy, L.A. Crum, Bjerknes force and bubble levitation under single-bubble sonoluminescence conditions, J. Acoust. Soc. Am. 102 (1997) 1522–1527.
[24] Y. Zhang, Z. Zhang, J. Wu, Y. Liu, M. Zhang, C. Yang, M. He, X. Gong, Z. Zhang, Z. Wang, F. Li, Study on fracture of tungsten wire induced by acoustic cavitation at different hydrostatic pressures and driving electric powers, Ultrason. Sonochem. 68 (2020) 105232, https://doi.org/10.1016/j.ultsonch.2020.105232.
[25] D. Song, W. Xu, M. Luo, M. Zhang, H. Wen, X. Cheng, X. Luo, Z. Wang, Influence of carbon nano-dots in water on sonoluminescence, Nanoscale (2021), https://doi.org/10.1039/d1nr02194j.
[26] P. Kanthale, M. Ashokkumar, F. Grieser, Sonoluminescence, sonochemistry (H2O2 yield) and bubble dynamics: frequency and power effects, Ultrason. Sonochem. 15 (2008) 143–150, https://doi.org/10.1016/j.ultsonch.2007.03.003.
[27] N.V. Kiassen, D. Marchington, H.C.E. McGowan, H_20_2 determination by the I_3^- method and by KMn04 titration, Angew. Chem. Int. Ed. 66 (1994) 2921–2925.
[28] Z. Galavani, R. Rezaei-Nasirabad, S. Bhattarai, On the dynamics of moving single bubble sonoluminescence, Phys. Lett. Sect. A Gen. At. Solid State Phys. 374 (2010) 4531–4537, https://doi.org/10.1016/j.physleta.2010.09.017.
[29] G.L. Sharipov, B.M. Gareev, A.M. Abdrakhmanov, Confirmation of hydrated electrons formation during the moving single-bubble sonolysis: activation of Tb3+ ion sonoluminescence by eaq- acceptors in an aqueous solution, J. Photochem. Photobiol. A Chem. 402 (2020), 112800, https://doi.org/10.1016/j.jphotochem.2020.112800.
[30] A. Troia, D.M. Ripa, R. Spagnolo, Moving single bubble sonoluminescence in phosphoric acid and sulphuric acid solutions, Ultrason. Sonochem. 13 (2006) 278–282, https://doi.org/10.1016/j.ultsonch.2005.06.002.
[31] J.R. Blake, T.J. Matula, Inertial cavitation and single-bubble sonoluminescence, Philos. Trans. R. Soc. A Math. Phys. Eng. Sci. 357 (1999) 225–249, https://doi.org/10.1098/rsta.1999.0325.
[32] A. Prosperetti, A new mechanism for sonoluminescence, J. Acoust. Soc. Am. 101 (1997) 2003–2007, https://doi.org/10.1121/1.418133.
[33] W.C. Moss, D.B. Clarke, D.A. Young, Calculated pulse widths and spectra of a single sonoluminescing bubble, Science (80-) 276 (1997) 1398–1401.
[35] W.F. Chan, G. Cooper, C.E. Brion, Absolute optical oscillator strengths for the electronic excitation of atoms at high resolution: experimental methods and measurements for helium, Phys. Rev. A 44 (1991) 186–204.
[36] K. Yasui, Single-bubble and multibubble sonoluminescence, Phys. Rev. Lett. 83 (1999) 4297–4300, https://doi.org/10.1103/PhysRevLett.83.4297.
[37] S. Chen, Y. Huang, B. Cai, Normal distribution of confinement energy from a photoluminescence line shape analysis in oxidized porous silicon, Solid State Electron. 49 (2005) 940–944.
[38] J.H. Bang, K.S. Suslick, Applications of ultrasound to the synthesis of nanostructured materials, Adv. Mater. 22 (2010) 1039–1059, https://doi.org/10.1002/adma.200904093.
[39] E.L. Mead, R.G. Sutherland, R.E. Verrall, The effect of ultrasound on water in the presence of dissolved gases, Can. J. Chem. 54 (1976) 1114–1120, https://doi.org/10.1139/v76-159.
[40] Y.T. Didenko, S.P. Pugach, Optical spectra of water sonoluminescence, Ultrason. Sonochem. 1 (1994) S9–S12, https://doi.org/10.1016/1350-4177(94)90019-1.
[41] Y.T. Didenko, T.V. Gordeychuk, Multibubble sonoluminescence spectra of water which resemble single-bubble sonoluminescence, Phys. Rev. Lett. 84 (2000) 5640–5643.
[42] J. Schneider, R. Pflieger, S.I. Nikitenko, D. Shchukin, H. Möhwald, Line emission of sodium and hydroxyl radicals in single-bubble sonoluminescence, J. Phys. Chem. A 115 (2011) 136–140.
[43] R. Pflieger, T. Ouerhani, T. Belmonte, S.I. Nikitenko, Use of NH (A3Π-X3Σ-) sonoluminescence for diagnostics of nonequilibrium plasma produced by multibubble cavitation, Phys. Chem. Chem. Phys. 19 (2017) 26272–26279, https://doi.org/10.1039/C7CP04813K.
[44] D. Qu, Z. Sun, M. Zheng, J. Li, Y. Zhang, G. Zhang, H. Zhao, X. Liu, Z. Xie, Three Colors Emission from S,N Co-doped Graphene Quantum Dots for Visible Light H2 Production and Bioimaging, Adv. Opt. Mater. 3 (2015) 360–367. https://doi.org/https://doi.org/10.1002/adom.201400549.
[45] H. Ding, S.B. Yu, J.-S. Wei, H.M. Xiong, Full-color light-emitting carbon dots with a surface-state-controlled luminescence mechanism, ACS Nano 10 (2016) 484–491, https://doi.org/10.1021/acsnano.5b05406.
[46] K.-H. Wu, Y. Liu, J. Luo, B. Wang, J. Xu, C. Pham-Huu, D. Su, The coulombic nature of active nitrogen sites in N-doped nanodiamond revealed in situ by ionic surfactants, ACS Catal. 7 (2017) 3295–3300, https://doi.org/10.1021/acscatal.7b00579.
[47] Y. Li, H. Liu, X.-Q. Liu, S. Li, L. Wang, N. Ma, D. Qiu, Free-radical-assisted rapid synthesis of graphene quantum dots and their oxidizability studies, Langmuir 32 (2016) 8641–8649, https://doi.org/10.1021/acs.langmuir.6b02422.
[48] C.R. Hill, J.C. Bamber, G.R. Ter Haar, Therapeutic and Surgical Applications, John Wiley & Sons Ltd, 2004.
[49] A.A. Doinikov, Acoustic radiation forces: classical theory and recent advances, Transw. Res. Netw. India Recent Res. Devel. Acoust. 37661 (2003) 39–67.
[50] Y. Xu, M. Wu, X.Z. Feng, X.B. Yin, X.W. He, Y.K. Zhang, Reduced carbon dots versus oxidized carbon dots: photo- and electrochemiluminescence investigations for selected applications, Chem. - A Eur. J. 19 (2013) 6282–6288, https://doi.org/10.1002/chem.201204372.
[51] D.J. Flannigan, K.S. Suslick, Emission from electronically excited metal atoms during single-bubble sonoluminescence, Phys. Rev. Lett. 99 (2007) 1–4, https://doi.org/10.1103/PhysRevLett.99.134301.
[52] M. Acik, G. Lee, C. Mattevi, A. Pirkle, R.M. Wallace, M. Chhowalla, K. Cho, Y. Chabal, The role of oxygen during thermal reduction of graphene oxide studied by infrared absorption spectroscopy, J. Phys. Chem. C 115 (2011) 19761–19781, https://doi.org/10.1021/jp2052618.
[53] S.I. Nikitenko, P. Martinez, T. Chave, I. Billy, Sonochemical disproportionation of carbon monoxide in water: evidence for Treanor effect during multibubble cavitation, Angew. Chem. - Int. Ed. 48 (2009) 9529–9532, https://doi.org/10.1002/anie.200904275.
[54] A. Gaydon, The Spectroscopy of Flames, 1974. https://doi.org/10.1007/978-94-009-5720-6_13.
[55] A.C. Le Floch, C. Amiot, Fourier transform spectroscopy of the CO Ångström bands, Chem. Phys. 97 (1985) 379–389.
[56] R. Pflieger, E. Fayard, C. Noel, S.I. Nikitenko, T. Belmonte, Molecular emissions in sonoluminescence spectra of water sonicated under Ar-based gas mixtures, Ultrason. Sonochem. 58 (2019) 104637, https://doi.org/10.1016/j.ultsonch.2019.104637.
[57] P.K. Carroll, Structure of the triplet bands of CO, J. Chem. Phys. 36 (1962) 2861–2869, https://doi.org/10.1063/1.1732392.
[58] M. Momona, H. Kanamori, K. Sakurai, High-resolution study of the perturbation in the CO triplet band, J. Mol. Spectrosc. 159 (1993) 1–16, https://doi.org/10.1006/jmsp.1993.1099.
[59] N.C. Eddingsaas, K.S. Suslick, Evidence for a plasma core during multibubble sonoluminescence in sulfuric acid, J. Am. Chem. Soc. 129 (2007) 3838–3839.